Available online at www.sciencedirect.com
SCIENCE DIRECT®
Journal of Membrane Science 237 (2004) 51–59
journal of MEMBRANE SCIENCE
www.elsevier.com/locate/memsci

# A Monte Carlo simulation model for membrane distillation processes: direct contact (MD)

A.O. Imdakm*, T. Matsuura

*Department of Chemical Engineering, Industrial Membrane Research Institute, University of Ottawa, Ottawa, Canada K1N 6N5*

Received 19 September 2003; received in revised form 30 January 2004; accepted 9 March 2004

**Abstract**

Direct contact membrane distillation (DCMD) has a great potential for applications in many areas of separation processes. Usually, in these processes, water constitutes a major component in fluid permeation, which is caused by the temperature difference between the feed and permeate. The transport models that are found in the literature in association with this process are often based on the Dusty-Gas model (DGM) for gas transport through porous media. These models' predictions are restricted to those cases in which only molecular diffusion and/or viscous flow contribute to the transport process. In this paper, a Monte Carlo simulation model is developed to study vapor permeation through membrane pores in association with DCMD. A three-dimensional network of interconnected cylindrical pores with a pore size distribution represents the porous membrane. The model takes also into account all molecular transport mechanisms based on the kinetic gas theory for a single cylindrical tube. The mechanisms are further dictated by the mean free path of permeating vapor molecules, by the size of the pores and by the operating conditions. Therefore, this model is comprehensive in its approach and can be applied to all forms of membrane distillation (MD) processes without resorting to any adjustable parameters. Model prediction(s) are in good qualitative agreement with available experimental data.


*Keywords:* Direct contact; Membrane distillation; Monte Carlo; Micro-porous hydrophobic membrane; Network model

## 1. Introduction

Direct contact membrane distillation (DCMD) is a thermally driven separation process, in which liquid feed and liquid permeate are in direct contact with the membrane surfaces, the deriving force being the vapor pressure gradient generated by temperature difference imposed between the two membrane sides. This process is one form of membrane distillation (MD) processes; it uses hydrophobic micro-porous membranes and operates on the principle of vapor–liquid equilibrium (VLE) conditions. Volatile components in the feed solution evaporate at the membrane pore entrance (feed side); permeate through pores by diffusion and/or convection, while non-volatile components such as colloids, macromolecules and electrolytes remain in the feed solution. The hydrophobic nature of the porous membranes prevents the penetration of feed solution into the membrane pores.

Attempts have been made to apply this process in many areas of scientific and industrial interest, yielding highly purified permeate and separating contaminants from liquid solutions; e.g. it has been applied in water desalination [1,2], wastewater treatment in textile [3] and pharmaceutical industry [4], and in the treatment of thermally sensitive industrial products such as concentrating aqueous solutions in fruit juices [5,6].

DCMD separation process should be characterized by both simultaneous heat and mass transfer, since mass (vapor) transport through membrane pores occurs as a result of the difference in temperature and composition between the feed and the permeate. Vapor flux across the DCMD membrane was described in the literature by two different models; i.e. the "Dusty-Gas" model (DGM) [12] and a model proposed by Schofield et al. [13–15]. In both of these models, vapor flux across membrane pores was described by the kinetic theory of gas transport. In the Dusty-Gas model [7–10], the porous media in general is visualized as an assembly of immobile spherical molecules, where the transport of vaporous molecules occurs by three mechanisms

* Fax: +1-613-562-5172.
*E-mail address:* abdussalam_o@hotmail.com (A.O. Imdakm).

0376-7388/$ – see front matter © 2004 Elsevier B.V. All rights reserved.
doi:10.1016/j.memsci.2004.03.005

[11]. In each mechanism, a molecule loses momentum in the direction of flow; i.e. the first is due to direct collisions with a capillary wall (Knudsen), the second due to collisions of unlike molecules (molecular) and the third due to indirect contact with capillary walls via molecule–molecule collisions terminating at molecule-wall collisions (viscous). The general expression of DGM applicable to DCMD process involves three adjustable parameters that are ordinary, binary and Knudson diffusivities. When the average membrane pore size is comparable to the molecular mean free path length ($\lambda$), i.e. ($\langle D_{\text{pore}} \rangle \approx \lambda$), surface and ordinary diffusion can be neglected and the general form of DGM falls into Knudson–viscous transition region. In this case, the total pressure drop is due to the sum of two momentum transfer processes discussed above; one is (Knudson resistance), while the other (viscous resistance). The expression for vapor flux across porous membrane based on the DGM can be re-written as [12]:

$$N_i = \frac{-1}{RT_{\text{avg}}} \left[ K_{\text{o}} \left( \frac{8RT_{\text{avg}}}{\pi M_i} \right)^{1/2} \nabla p_i + B_{\text{o}} \frac{p_{i,\text{avg}}}{\mu} \nabla P \right], \quad (1)$$

where $N_i$ and $M_i$ are the molar flux and the molecular weight, respectively, of species $i$, $P$ the total pressure, $\nabla p_i$ the gradient in the partial pressure of $i$th species, $T_{\text{avg}}$ the average membrane temperature, $\mu$ the transporting fluid viscosity, and $R$ the gas constant. $K_{\text{o}}$ and $B_{\text{o}}$ are constants that can be calculated from gas permeation experimental data of non-condensable pure gas such as nitrogen, helium, or air [12,20].

The other model was developed by Schofield et al. [13,14]. This model is based on the assumption that in the transition region between the Knudson and viscous flows, the permeability of the porous medium (membrane) can be considered as a linear combination of Knudson and viscous permeabilities; the proposed model is approximated as:

$$N \approx -aP_{\text{r}}^{\text{b}} \Delta P \quad (2)$$

where $\Delta P$ is the pressure drop across the membrane, $N$ the molar flux, and the exponent $b$ lies between 0 and 1, depending on the extent of viscous flow contribution. $P_{\text{r}} \approx 1$ and it is a dimensionless pressure defined as $P_{\text{avg}}/P_{\text{ref}}$, where $P_{\text{ref}}$ is chosen in such a way that $P_{\text{r}}$ becomes close to unity for the range of application. And $a = K/\delta$ evaluated at $P_{\text{ref}}$, with $K$ being the permeability defined as $K = -N\delta/\Delta P$ where $\delta$ is the membrane thickness. In this model, the parameters ($a$ and $b$) depend on the reference pressure chosen and upon the gas used.

The objective of this investigation is to develop a Monte Carlo simulation model to describe the performance of the DCMD separation process and to predict vapor flux across the membrane (permeability). A three-dimensional network of interconnected pores with a pore size distribution represents the porous membrane. This model uses gas transport mechanisms developed by the kinetic theory of gases. These gas transport expressions can describe vapor flux through the entire range of the membrane pore size distribution. The applicability of each transport mechanism to describe the transport through each membrane pore depends on the size of the pore, the mean free path length ($\lambda$) of the permeating molecule, and average pressure and temperature in the membrane pore. This model differs significantly from previous models employed by many investigators, because it takes into account the membrane pore size distribution, the appropriate transport mechanism governing vapor flux through each pore, pore space topology (connectedness) and the interconnection between membrane pores without resorting to any adjustable parameters. Once steady-state pressure and temperature distribution through the entire network node (site) is established, the vapor permeability of the simulated process can be evaluated. As such, this model is comprehensive and its applicability in describing transport through MD processes, we believe, is beyond the specific DCMD problem that we discuss as examples in this paper.

## 2. Theory

Experimental and theoretical studies found in the literature relate molecular transport in MD processes to the kinetic theory of gases. Accordingly, the vapor transport mechanism depends upon the mean free path length ($\lambda$), which can be calculated based on the average process operating conditions (pressure and temperature), and the average size of the membrane pores ($\langle D_{\text{pore}} \rangle$). The value of $\lambda$, defined as the average distance the molecule of diffusing species travels between two successive collisions, can be calculated from the kinetic theory of gases by the following equation [16]:

$$\lambda = \frac{k_{\text{B}} T}{P\sqrt{2}\pi\sigma^2} \quad (3)$$

where $k_{\text{B}}$ is the Boltzmann constant, $T$ the absolute temperature (K), $P$ the total pressure (Pa) and $\sigma$ the collision diameter (m). The mean free path length therefore is proportional to temperature and inversely proportional to pressure. In this study, the average temperature, $T_{\text{p,avg}}$ and average pressure, $P_{\text{p,avg}}$, in the pore are used as $T$ and $P$ in Eq. (3) [16]. Therefore, $\lambda$ is calculated for each pore of the entire pore network.

Considering $\lambda_i$ for $i$th species in a vaporous mixture and a pore with a diameter, $D_{\text{pore}}$, when $\lambda_i < D_{\text{pore}}$ the transport mechanism is the classical viscous (Poiseuile) flow and the molar flux, $N_{i\text{v}}$, of this species through the pore is given by

$$N_{i\text{v}} = -\frac{p_i r^2}{8RT\mu} \nabla P \quad (4)$$

where $p_i$ is the partial pressure of species $i$, $P$ the total pressure, $R$ the gas constant, $T$ the absolute temperature and $r$ the pore radius. When $\lambda_i > D_{\text{pore}}$ the transport mechanism is Knudsen flow and the molar flux, $N_{i\text{k}}$, is given by

$$\frac{N_{i\text{k}}}{D_{i\text{k}}} = -\frac{1}{RT} \nabla p_i \quad (5)$$

where $\nabla p_i$ is the partial pressure gradient of species $i$ and $D_{i\mathrm{k}}$ the Knudson diffusion coefficient, which is given by

$$D_{i\mathrm{k}} = \frac{2}{3} r \left( \frac{8RT}{\pi M_i} \right)^{1/2} \tag{6}$$

where $M_i$ the molecular weight of species $i$. Again, average values for the pressures and temperature in the pore should be used in the above equations [16].

There are two other mechanisms for transport through pores; one is the transport of vapor by mutual diffusion, which takes place when $D_{\mathrm{pore}}$ is much larger than $\lambda$, and the other is the transport by surface flow, which takes place when $D_{\mathrm{pore}} < 0.02\,\mu\mathrm{m}$ [21,22]. The last two mechanisms are usually ignored in DCMD, since DCMD is usually carried out under relatively low pressure, which means $\lambda$ is relatively large, and with pore sizes in a range $0.1 < D_{\mathrm{pore}} < 1\,\mu\mathrm{m}$ [12]. It should be noted out that in desalination of sea and brackish water and dehydration of sugar solutions, water is the only permeate. In such cases, the total pressure $P$ in the above equations can replace the partial pressure $p_i$.

Concerning the total vapor pressure, $P$, with the assumption made that MD process operates on the principle of vapor–liquid equilibrium conditions, VLE data or equations can be used to calculate water vapor pressure when the solute concentration in the aqueous solution is low and the solution is well degassed. In this study, the saturation vapor pressure of water, $P$, is estimated by the Antoine equation [12,20,23]:

$$P = \exp\left[ A - \frac{B}{C + T} \right], \tag{7}$$

where $A$, $B$ and $C$ are 23.238, 3841 and −45, respectively, for water [23]. As a result, Eq. (7) is applied to determine the water vapor pressure at both side of the membrane (interfacial) from the given feed and permeate interfacial temperature. This gives process vapor flux boundary conditions. As well, it is used to calculate the temperature distribution (nodal temperature) from the vapor pressure distribution (nodal vapor pressure) and vice versa. (To know the pressure distribution means to know the pressure value at each node. The meaning of temperature distribution is the same.)

## 3. Model formulation

A porous membrane is represented by a simple-cubic network The bonds of the network which represent the membrane pore throats, are assumed to be cylindrical capillary tubes of effective radii $R_{\mathrm{pore}}$ and a constant length $l$ (see Fig. 1). The effective pores diameter, $D_{\mathrm{pore}}$, are distributed according to a statistical distribution function, which is in this paper, assumed to be a log-normal probability density function with a geometric mean pore size of $\mu_{\mathrm{pore}}$ and a standard deviation $\sigma_{\mathrm{pore}}$. This distribution mimics qualitatively pore size distributions determined experimentally by several

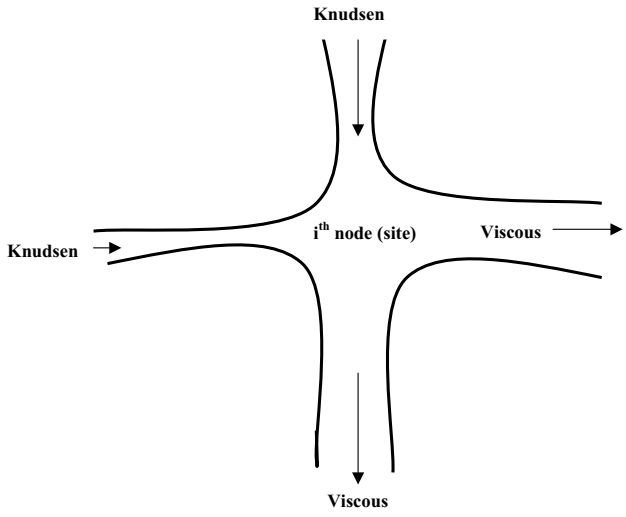


Fig. 1. Vapor flux transport mechanisms during membrane distillation, DCMD.

investigators [18,19]. However, any other type of pore size distribution can be used, if necessary:

$$\frac{\mathrm{d}\, f(D_{\mathrm{pore}})}{\mathrm{d}\, D_{\mathrm{pore}}} = \frac{1}{D_{\mathrm{pore}} (\ln \sigma_{\mathrm{pore}}) \sqrt{2\pi}} \exp\left[ - \frac{(\ln D_{\mathrm{pore}} - \ln \mu_{\mathrm{pore}})^2}{2 (\ln \sigma_{\mathrm{pore}})^2} \right] \tag{8}$$

The geometric mean pore sizes and the standard deviations for three membranes (A, B and C) used in this investigation and the corresponding probability density curves are given in Fig. 2. The sites (nodes) of the network, which represent the membrane pore bodies, are assumed to be large enough in order to able to contain the transporting molecules but the effect of their sizes on the pressure and temperature fields is ignored.

A three-dimensional network model used in this study was $L \times L \times L$ (simple-cubic), where $L = 12$, i.e., the network has 12 nodes (sites) in every direction plus boundary conditions sites (feed and permeate). The pore length $l$ is assumed to be a constant length (1.0 μm), but it could have any value evaluated experimentally or theoretically [17].

Once the geometrical configuration, i.e. pore size and length $l$, is given to the pore network, one can calculate the effective pressure field and the temperature field through the entire network and its effect on the vapor flux through the membrane. The calculation procedure is as follows.

### 3.1. Calculation of pressure and temperature distribution

In order to calculate pressure and temperature distribution at each network node (site), one has to calculate the mass flux through each pore which is given as $J_{ij} = C_{ij} M_i \Delta P_{ij}$, where $\Delta P_{ij}$ the pressure difference across the $ij$th pore and $C_{ij}$ the mass conductance coefficient of this pore. For pores dominated by viscous flow transport mechanism $C_{ij}$ is de-

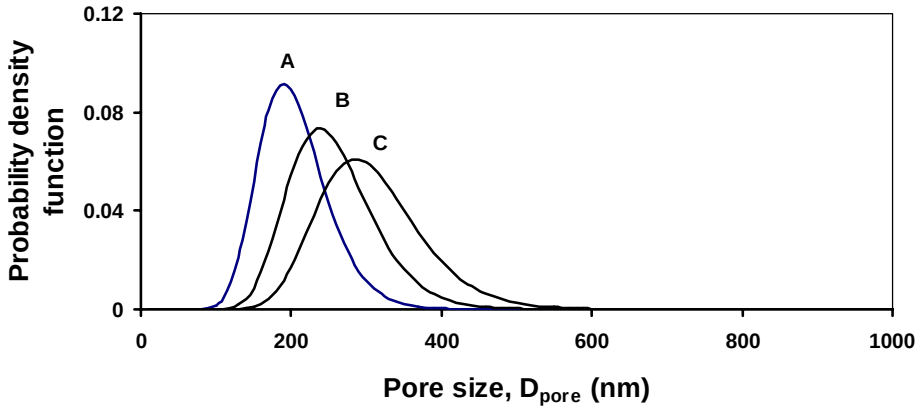


Fig. 2. Probability density function curves for membranes A ($\mu_p = 200$ nm), B ($\mu_p = 250$ nm) and C ($\mu_p = 300$ nm), with a constant $\sigma_p = 1.25$.

fined as $C_{ijv}$, but for pores dominated by Knudsen transport mechanism, it is defined as $C_{ijk}$. Other forms of the vapor transport mechanism such as surface and molecular diffusion can be included; however, they are neglected in this investigation, as stated earlier. Substituting $\nabla P$ for $\Delta P/l$ and multiplying the cross-sectional area $\pi r^2$, from Eqs. (4) and (5) become

$$C_{ijv} = \frac{P_{p,avg}\pi r^4}{8RT_{p,avg}\mu l} \tag{9}$$

and

$$C_{ijk} = -\frac{2}{3l}\left(\frac{8\pi}{RT_{p,avg}M_i}\right)^{1/2} r^3 \tag{10}$$

respectively, where $\mu$ is the fluid viscosity. As explained earlier, the average pressure and temperature in the pore, $P_{p,avg}$ and $T_{p,avg}$, are used for the pore $ij$ [16]. A mass balance for each node of the entire network, assuming the transport of pure substance, in this case water vapor only, gives

$$\sum_j C_{ij}\Delta P_{ij} = 0 \tag{11}$$

where $\Delta P_{ij}$ is the pressure drop across the pore, $C_{ij}$ as defined above and the sum is over all pores $ij$'s that are connected to the $i$th node. Writing down Eq. (11) and substituting a proper $C_{ij}$ for each node $i$ of the network gives a set of simultaneous equations. These equations are solved with boundary conditions that are constant mass flux ($J_{ij}$) imposed at network entrance ($Z = 0$, feed) and network exit ($Z = L + 1$, permeate), and matched with periodic boundary conditions in the $X$ and $Y$ directions.

Vapor pressure and temperature at each node can be computed iteratively using proper iterative method such as method of successive substitution and/or Newton–Raphson method [26]. As an initial guess for the iterative procedure, a linear vapor pressure change from $Z = 0$ to $L + 1$ is assumed. The corresponding nodal initial temperature can be calculated by using the Antoine equation. Once the vapor pressure and temperature are evaluated at each network node (site), molecular mean free path lengths ($\lambda$) can be calculated based on the average pressure and temperature in the pore. Hence $C_{ij}$ can be calculated using Eq. (9) or Eq. (10). Writing down Eq. (11) for each node $i$ of the entire network and with the proper $C_{ij}$ give a set of simultaneous equations of nodal pressure that can be solved iteratively as mentioned above. Then, the corresponding temperature distribution is calculated from the Antoine equation.

The vapor pressure field so computed at the $n$th iteration is compared with the vapor pressure field computed at $(n-1)$th iteration. If the difference in vapor pressure between $n$th iteration and $(n-1)$th iteration exceeds two percent (2%) at any node (site) of the entire network, the whole vapor pressure field is re-calculated as discussed above. Once the differences between the two consecutive steps become below 2%, we assume that the vapor pressure and the corresponding temperature are the steady-state values. One can calculate DCMD vapor flux as the sum of the vapor flux of each entering pore, $\sum J_{in}$, at the membrane feed side or the sum of vapor flux of each exiting pore, $\sum J_{out}$, at the membrane permeate side, taking into account the proper vapor flux transport mechanism governing each pore.

## 4. Results and discussion

In this study, an extensive Monte Carlo simulation of DCMD process has been carried out to evaluate vapor flux (permeability) under different operating condition(s) for three membranes (A, B and C, see Fig. 2) with different pore sizes and pore size distributions. This study was carried out at different feed bulk interfacial temperatures, while the temperature on the permeate side was held constant at 20 °C.

In Fig. 3, the results of vapor flux calculation in which only the Knudsen diffusion mechanism was included are shown for different feed temperature. The figure shows that model predictions are in good qualitative agreement with experimental data [24]. In Figs. 4–6 viscous flow mechanism was included and calculations were made under the conditions same as Fig. 3. From Figs. 4–6, it is obvious that the

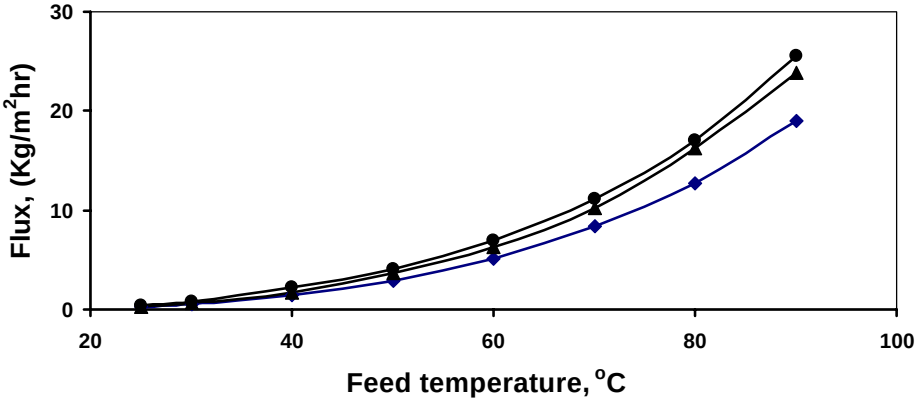


Fig. 3. Simulated DCMD vapor flux. Process is controlled by Knudsen diffusion mechanism only. (■) Membrane A, (▲) membrane B, (●) membrane C.

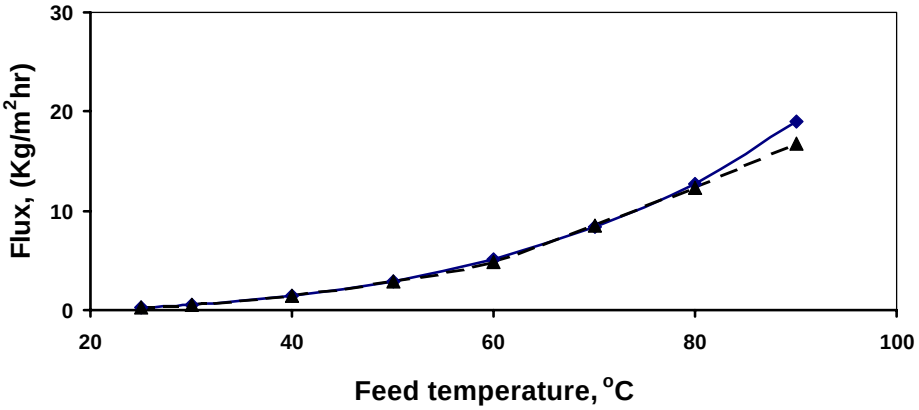


Fig. 4. Comparison of simulated DCMD vapor flux for membrane A. (■) Process is controlled by Knudsen diffusion mechanism only; and (▲) by Knudsen diffusion and viscous flow mechanisms.

flux decreases significantly when viscous flow is included. The decrease in vapor flux occurs only when the feed temperature is more than 70 °C and becomes more significant with an increase in the feed temperature. The vapor flux decline is also enhanced by an increase in the means pore size from membrane A to C.

The above observation can be better understood by knowing the fraction of pores where viscous flow takes place. Fig. 7 shows the fraction of such pores as a function of the feed temperature for the three different membranes. The figure shows that the change from Knudsen diffusion to viscous flows occurs more when the feed temperature increases and the mean pore size increases from A to C, which seems quite natural. Fig. 8 shows the fraction of pores where the viscous flow occurs as a function of the distance from the feed/membrane interface in the direction of flow. The figure

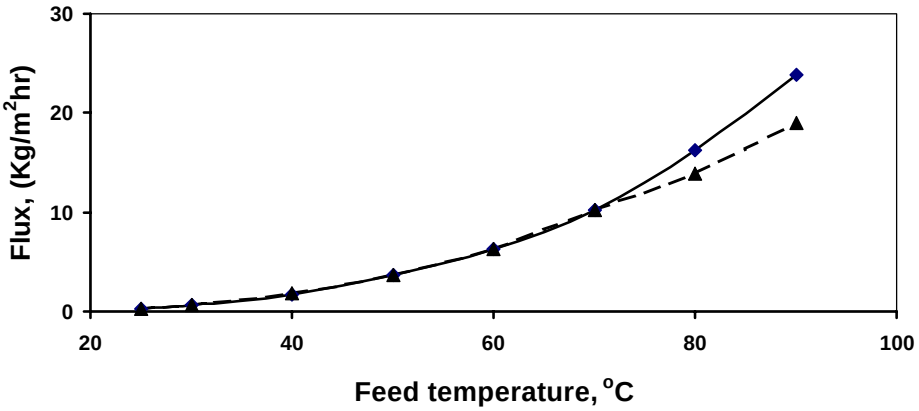


Fig. 5. Comparison of simulated DCMD vapor flux for membrane B. (■) Process is controlled by Knudsen diffusion mechanism only; and (▲) by Knudsen diffusion and viscous flow mechanisms.

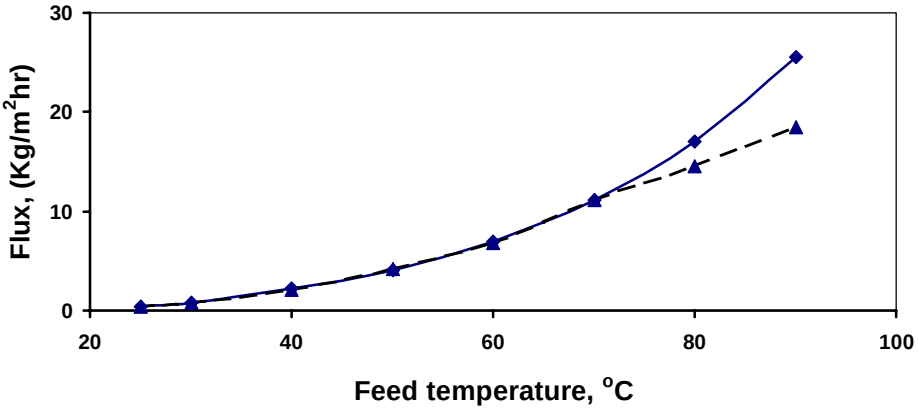


Fig. 6. Comparison of simulated DCMD vapor flux for membrane C. (■) Process is controlled by Knudsen diffusion mechanism only; and (▲) by Knudsen diffusion and viscous flow mechanisms.

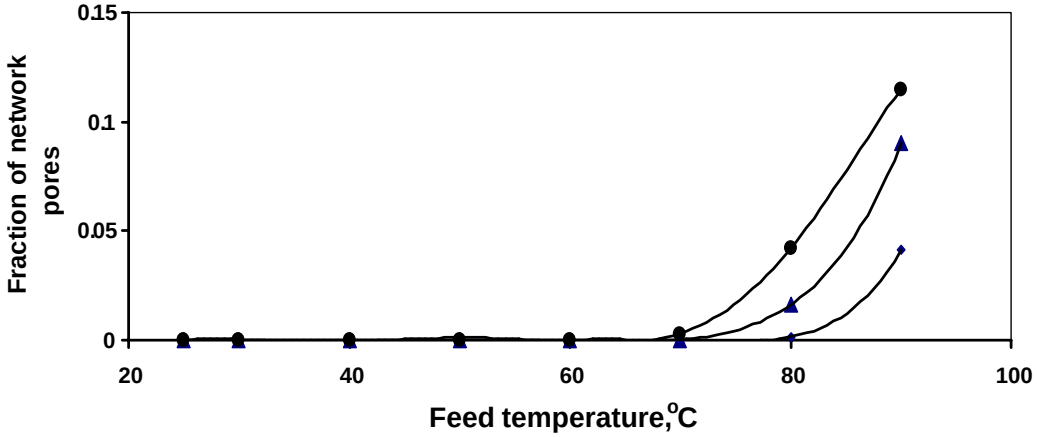


Fig. 7. Effect of the feed temperature and the membrane pore size distribution on the fraction of pores governed by viscous flow. (■) Membrane A, (▲) membrane B, (●) membrane C.

shows that most of the viscous flow occurs near the interface. Approximately, 90% of the pores where the viscous flow occurs are limited to the first two layers of pores. Note that the first layer (1) is in direct contact with the feed. As we move away from the feed/membrane interface, the effect of viscous flow diminishes rapidly and disappears at the fifth layer.

Thus, the decrease in vapor flux reduction observed when viscous flow is included in the simulation can be interpreted in the following way. Note that the flux due to the viscous flow is less than that due to the Knudsen diffusion. When the temperature of the feed solution is increased, the vapor pressure at the feed/membrane interface (network entrance) increases non-linearly, leading to the reduction in the mean free path length, $\lambda$. This reduction further results in shift from the Knudsen diffusion to viscous flow in some pores. This shift occurs more near the feed/membrane interface and less as you go down in the vapor flow direction.

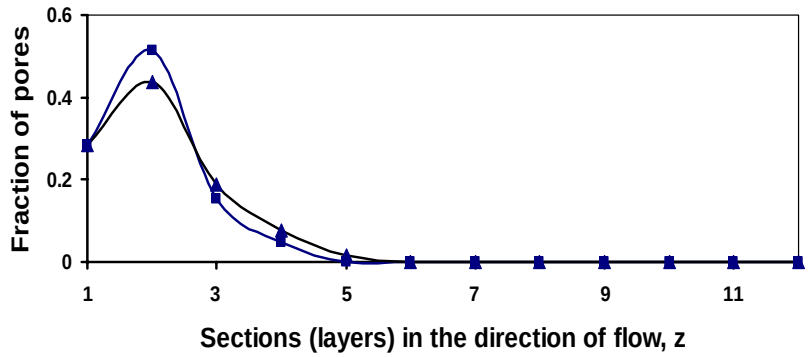


Fig. 8. Distribution of pores governed by viscous flow in the direction of macroscopic flow. Feed temperature: (■) 80 °C and (▲) 90 °C.

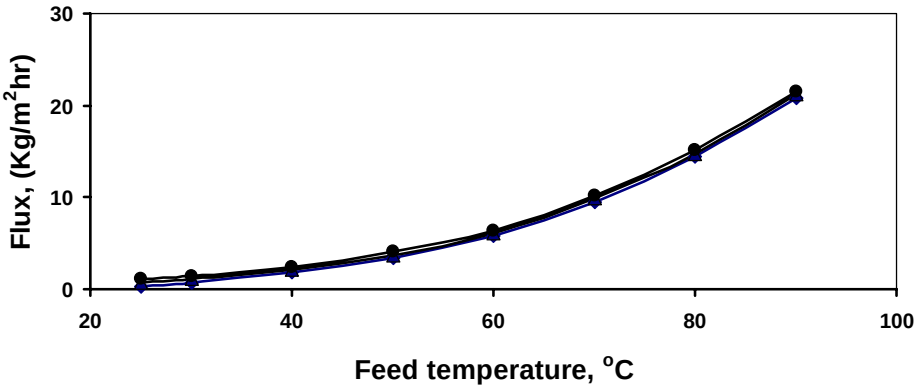


Fig. 9. Effect of pressure reduction at the permeate side on the vapor flux. Process is controlled by Knudsen diffusion mechanism only (membrane B). (■) 0% reduction, (▲) 50% reduction, (●) 95% reduction.

To study the effect of vapor pressure reduction on the permeate side on the vapor flux, a simulation was carried out at the following three different permeate pressures using membrane B: (1) at a permeate pressure corresponding to the water vapor pressure at 20 °C, (2) at a permeate pressure 50% lower than the first case, (3) at a permeate pressure 95% lower then the first case. Note that the last case is similar to vacuum membrane distillation (VMD). First, simulation was done without including the viscous flow and the results given in Fig. 9. The figure shows that the effect of permeate pressure reduction is not significant. In fact, the fluxes for the three cases were almost the same when feed temperature is above 70 °C. These results show that the change of the vapor pressure gradient alone does not affect significantly the over all vapor flux. This maybe related to the permeate temperature as low as 20 °C and the corresponding vapor pressure which is already very low. Hence, further decrease in permeates pressure will not affect significantly the pressure gradient, resulting in insignificant change in process vapor flux.

When the viscous flow contribution is included, on the other hand, the increase in vapor flux caused by the decrease in permeate pressure is rather significant, as demonstrated in Fig. 10. This is because, in addition to an increase in the vapor pressure gradient as mentioned above, the shift (Knudsen diffusion ↔ viscous flow) is involved in the latter simulation. When the permeate pressure is lowered, Knudsen diffusion occurs in a larger number of pores, resulting in an increase in the overall membrane vapor flux.

Fig. 11 shows the effect of permeate side pressure reduction on the fraction of membrane pores governed by viscous flow. This figure indicates that the relative increase in vapor flux (Fig. 10) is in fact due to the decrease in the number of pores governed by viscous flow. Furthermore, because of relatively low vapor pressure at the permeate side, the shift from viscous to Knudsen diffusion is only marginal and it may occur in the pores located far down from the feed/membrane interface (the network entrance); i.e. in close vicinity to permeate side and/or at pores of relatively small pore sizes. Because of the location of and the size, those pores have only a limited role to play on the overall vapor flux.

The influence of vapor pressure reduction at the permeate side would become more significant as the temperatures at the feed and the permeate side of the membrane becomes closer. This is because both the pressure gradient across the membrane and the shift from viscous flow to Knudsen diffusion will be enhanced more strongly. Moreover, the latter shift will occur in pores of relatively large sizes and also at

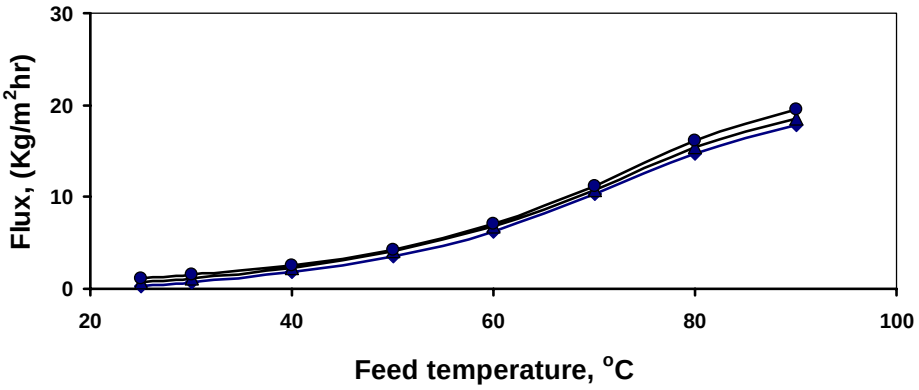


Fig. 10. Effect of pressure reduction at the permeate side on the vapor flux. Process is controlled by Knudsen diffusion and viscous flow mechanisms (membrane B). (■) 0% reduction, (▲) 50% reduction, (●) 95% reduction.

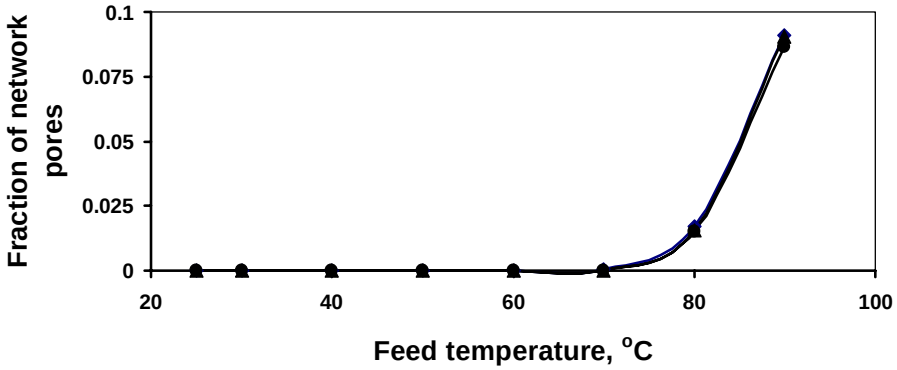


Fig. 11. Effect of the feed temperature and the permeate pressure reduction on the fraction of pores governed by viscous flow (membrane B). (■) 0% reduction, (▲) 50% reduction, (●) 95% reduction.

the pores in closer vicinity to the feed/membrane interface (pore network entrance). In such a case, the permeate vapor pressure reduction will cause a considerable increase in vapor flux across the membrane as it has been observed in many experimental studies carried out buy many VMD investigators [25]. These issues will be discussed in detail in future publications.

## 5. Summary

In this investigation, a Monte Carlo simulation model was developed to describe vapor flux for direct contact membrane distillation. A three-dimensional network of interconnected pores represents the porous membrane. Mass transfer in a single capillary founded on the kinetic gas theory describes the vapor flux at each pore. The results obtained are in good qualitative agreement with the available experimental data [24]. The model is general in its approach, and is applicable to a wide class of problems of membrane distillation. The model can take into consideration at the pore level all possible features of transport mechanisms and boundary conditions that may affect MD process. The model can also represent the pore space realistically. As such it can be applied to all forms of MD processes. The ability of the model in predicting experimental data in MD processes will be discussed more in detail in future publications.

**Nomenclature**

| | |
|---|---|
| $B_o$ | viscous flux coefficient ($m^2$) |
| $C_{ij}$ | mass conductance of pore $ij$ |
| $D_{ik}$ | Knudsen diffusion coefficient ($m^2\,s^{-1}$) |
| $D_{pore}$ | pore diameter (m) |
| $J$ | mass flux ($kg\,m^{-2}\,h^{-1}$) |
| $J_{in}$, $J_{out}$ | pore vapor flux at network entrance or exit ($kg\,m^{-2}\,h^{-1}$) |
| $k_B$ | Boltzmann constant ($J\,K^{-1}$) |
| $K$ | membrane permeability ($mol\,m^{-2}\,h^{-1}\,Pa^{-1}$) |
| $K_o$ | Knudsen flux coefficient (m) |
| $l$ | pore length (m) |
| $L$ | network length (m) |
| $M_i$ | molecular weight of species $i$ ($kg\,mol^{-1}$) |
| $N$ | molar flux ($mol\,m^{-2}\,h^{-1}$) |
| $P$ | total pressure (Pa) |
| $P_i$ | partial pressure of species $i$ (Pa) |
| $P_{p,avg}$ | average pore pressure (Pa) |
| $R$ | gas constant ($J\,mol^{-1}\,K^{-1}$) |
| $R_{pore}$ | pore radius (m) |
| $T_{avg}$ | average membrane temperature (K) |
| $T_{p,avg}$ | average pore temperature (K) |
| $X$, $Y$, $Z$ | axial coordinate |
| *Greek letters* | |
| $\delta$ | membrane thickness (m) |
| $\lambda$ | mean free path (m) |
| $\lambda_i$ | mean free path of species $i$ (m) |
| $\mu$ | viscosity ($kg\,m^{-1}\,s^{-1}$) |
| $\mu_{pore}$ | mean pore size of the pores (m) |
| $\sigma_{pore}$ | geometrical standard deviation of the pores |

## References

[1] K. Schneider, W. Holz, R. Wollbeck, Membranes and modules for transmembrane distillation, J. Membr. Sci. 39 (1988) 25–42.
[2] R.W. Schofield, A.G. Fane, C.J.D. Fell, R. Macoun, Factors affecting flux in membrane distillation, Desalination 77 (1990) 279–294.
[3] V. Calabro, E. Drioli, F. Matera, Membrane distillation in textile wastewater treatment, Desalination 83 (1991) 209–224.
[4] Y. Wu, Y. Kong, J. Liu, J. Zhang, J. Xu, An experimental study on membrane distillation: crystallization for treating waste water in taurine production, Desalination 80 (1991) 235–242.
[5] S. Kimura, S. Nakao, Transport phenomena in membrane distillation, J. Membr. Sci. 33 (1987) 285–298.
[6] V. Calabro, B.L. Jiao, E. Drioli, Theoretical and experimental study on membrane distillation in the concentration of orange juice, Ind. Eng. Chem. Res. 33 (1994) 1803–1808.
[7] B.V. Deriagin, S.P. Bakanov, Theory of flow of a gas in a porous material in the near-Knudsen region, Tech. Phys. 2 (1957) 1904–1911.

[8] R.B. Evans, J. Truitt, G.M. Watson, Interdiffusion of helium and argon in a large-pore graphite, J. Chem. Eng. Data 6 (1961) 522–530.
[9] R.B. Evans, G.M. Watson, E.A. Mason, Gaseous diffusion in porous media a uniform pressure, J. Chem. Phys. 35 (1961) 2076–2083.
[10] E.A. Mason, A.P. Malinauskas, R.B. Evans, Flow and diffusion of gases in porous media, J. Chem. Phys. 46 (1967) 3199–3207.
[11] E.A. Mason, A.P. Malinauskas, Gas Transport in Porous Media: The Dust-Gas Model, Elsevier, Amsterdam, 1983.
[12] K.W. Lawson, D.R. Lloyd, Membrane distillation, J. Membr. Sci. 12 (1997) 1–25.
[13] R.W. Schofield, A.G. Fane, C.J.D. Fell, Gas and vapor transport through microporous membranes, I, Knudson Poiseuille transition, J. Membr. Sci. 53 (1990) 159–171.
[14] R.W. Schofield, A.G. Fane, C.J.D. Fell, Gas and vapor transport through microporous membranes, II, Membrane distillation, J. Membr. Sci. 53 (1990) 173–185.
[15] R.W. Schofield, A.G. Fane, C.J.D. Fell, Heat and mass transfer in membrane distillation, J. Membr. Sci. 33 (1987) 299–313.
[16] R.D. Present, Kinetic Theory of Gases, McGraw-Hill, New York, 1958.
[17] A.O. Imdakm, M. Sahimi, Computer simulation of particles transport processes in flow through porous media, Chem. Eng. Sci. 46 (1991) 1977–1993.
[18] Q.K. Wang, T. Matsuura, C.Y. Feng, M.R. Weir, C. Detellier, E. Rutadinka, R.L. Van Mao, The sepiolite membrane for ultrafiltration, J. Membr. Sci. 184 (2001) 153–163.
[19] S. Singh, K.C. Khulbe, T. Matsuura, P. Ramamurthy, Membrane characterization by solute transport and atomic force microscopy, J. Membr. Sci. 142 (1998) 111–127.
[20] C. Fernandez-Pineda, M.A. Izquierdo-Gil, M.C. Garcia-Payo, Gas permeation and direct contact membrane distillation experiment and their analysis using different models, J. Membr. Sci. 198 (2002) 33–49.
[21] Y. Fujii, S. Kigoshi, H. Iwatani, M. Aoyma, Selectivity and characteristics of direct contact membrane distillation type experiment, I, Permeability and selectivity through dried hydrophobic fine porous membrane, J. Membr. Sci. 72 (1992) 53–72.
[22] Y. Fujii, S. Kigoshi, H. Iwatani, M. Aoyma, Y. Fusaoka, Selectivity and characteristics of direct contact membrane distillation type experiment, II, Membrane treatment and selectivity increase, J. Membr. Sci. 72 (1992) 73–89.
[23] P.J. Fostor, A. Burgoyne, M.M. Vahdati, Improved process topology for membrane distillation, Sep. Purif. Technol. 21 (2001) 205–217.
[24] K.W. Lawson, D.R. Lloyd, Membrane distillation, II, Direct contact MD, J. Membr. Sci. 120 (1996) 123–1333.
[25] S. Bandini, A. Saavedra, G.C. Sarti, Vacuum membrane distillation experiments and modeling, AIChE J. 43 (1997) 398–408.
[26] R.G. Rice, D.D. Do, Applied Mathematics and Modeling for Chemical Engineers (Appendix A), Wiley, 1995.